IPP-Report

Max-Planck-Institut für Plasmaphysik

H. Saitoh, J. Horn-Stanja, E. Stenson, U. Hergenhahn,
T Sunn Pedersen, M. R. Stoneking

A note on levitation techniques toward construction of a superconducting levitated dipole experiment

IPP 17/52
August, 2016

A note on levitation techniques toward construction of a superconducting levitated dipole experiment

H. Saitoh[1], J. Horn-Stanja[1], E. Stenson[1], U. Hergenhahn[1], T. Sunn Pedersen[1], and M. R. Stoneking[2]
[1]*Max Planck Institute for Plasma Physics, Greifswald and Garching, Germany,* [2]*Lawrence University, Appleton, USA*
(Dated: August 29, 2016)

As one of magnetic confinement configurations for electron-positron pair-plasmas, the PAX/APEX team of IPP is conducting development studies on a compact levitated dipole experiment, APEX-D [1]. In this note, we describe basic knowledges needed for design and construction of magnetic field coils and its levitation system focusing on its practical aspects. We review mechanisms and techniques for the levitation of a superconducting dipole field coil, and then report development studies conducted at IPP. Based on these considerations, we plan to decide the machine design and optimize the parameters of the APEX-D as near future work. It is noted that most of concepts and ideas described in this note were developed by previous studies on levitated dipole experiments, or laboratory magnetospheres. Among these levitated dipole experiments, HS appreciates continuous support from the Mini-RT and RT-1 teams of The University of Tokyo in collaboration with NIFS.

I. INTRODUCTION

Closed magnetic field lines, which are suitable for the confinement of electron-positron plasmas [1], can be generated by a levitated dipole field coil [2]. In order to realize such a confinement configuration, we plan to develop and operate a compact superconducting (SC) levitated dipole experiment. Although SC coils are widely used in many physics experiments today, usage and operation of SC coils for the levitated dipole experiments [3, 4] are not very common. In these experiments, the SC dipole field coil must be levitated stably, and its persistent current must be sustained during experiments without cooling and external power supply. These operation schemes of SC coils might be quite unique among many experiments. Thus it would be useful to review basic concepts of levitation and to explain concise analysis and know-hows needed for the development of such systems. These levitation technologies have been developed in classical experiments conducted in 1970s, and they are attracting renewed interest after successful experiments at Mini-RT, RT-1 [5, 6], and LDX [7]. Based on these previous studies, we focus on basic concepts and practical considerations toward the development of a compact levitated dipole trap system for electron-positron plasma experiments.

Outline of this note is as follows. In Part I, we review the equilibrium and stability properties of a levitated magnet in the gravity and an electromagnetic force. In Sec. II, we define the coil model and review the dynamics and equilibrium of a levitated magnet (a permanent magnet and a SC coil). According to these analysis, we set first-step SC coil parameters suitable for the levitation operation. For these specific coil parameters, we numerically evaluate the behavior of coil motions, including the stability on vertical motion. In Sec. III, stabilities of the SC coil motions are studied in a view point of coil configuration. Here the coil motions are categorized into vertical, slide, and tilt motions. It will be shown that we can choose coil positions so that only vertical motion is unstable. Because the vertical motion is one dimensional, we can relatively easily control and stabilize this motion using an appropriate feedback system. It is noted that, in this analysis, the flux conservation effects of the SC are not considered. However, it will be shown that it is a good approximation for the equilibrium solution that will be used in APEX.

In Part II, we review feedback control system needed for the stabilization of vertical motion of a levitated coil. In Sec. V, the control system for the levitation is modeled and analyzed using transmission functions. We intend to stabilize the vertical motion by controlling the coil current of a levitation coil with a PID feedback system. Stabilization conditions are calculated numerically for such a system. In Sec. VI, we construct a mock-up experiment on the levitation system and demonstrate stable levitation of a permanent magnet, in order to verify the numerical analysis.

Part I: LEVITATION ANALYSIS

II. LEVITATION GEOMETRY AND EQUILIBRIUM

A. Definition of configuration and basic equations

As shown in Fig. 1, a floating SC coil (F coil) and a levitation coil (L coil) are located coaxially. The F coils is cooled down to a cryogenic temperature and then levitated around the equator ($z = 0$ m) position [4]. The L coil carries a total current of $I_\mathrm{L} \times N_\mathrm{L}$ (AT) which generates an attractive magnetic field force to levitate the F coil with a mass m_F (kg) and a total current of $I_\mathrm{F} \times N_\mathrm{F}$ (AT). The radii and vertical positions of two coils are (r_F, z_F) and (r_L, z_L), respectively. We denote the self inductances and mutual inductance between two coils as L_L, L_F, and M.

Coil motions in this system are decided by two basic equations. The first one is the equation of motion for the vertical motion of the F coil,

$$m\frac{d^2 z_\mathrm{F}}{dt^2} = -2\pi r_\mathrm{F} N_\mathrm{F} I_\mathrm{F} B_\mathrm{r} - m_\mathrm{F} g, \tag{1}$$

where B_r is the radial component of magnetic field at (r_F, z_F) generated by the L coil. Because B_r is proportional to I_L for a fixed geometry, we may write (1) as

$$m\frac{d^2 z_\mathrm{F}}{dt^2} = -2\pi r_\mathrm{F} N_\mathrm{F} h I_\mathrm{F} I_\mathrm{L} - m_\mathrm{F} g, \tag{2}$$

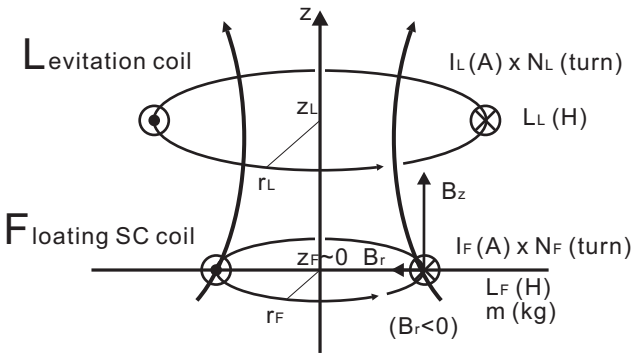

FIG. 1. Levitation model consisting of two coils carrying currents in the same direction. The floating (F) coil is levitated by the electromagnetic force between the F and the levitation (L) coils.

where

$$B_r(z) = h(z)I_L. \tag{3}$$

Another governing equation is on the flux conservation of a SC loop (fluxoid conservation). Because the total flux of a SC F coil is conserved, independent of the variation of I_F, the conservation law is

$$\frac{d}{dt}(L_F I_F + M I_L) = 0. \tag{4}$$

When I_L is constant, which is a good approximation for an equilibrium solution used in many levitated dipole experiments, we can reduce (4) as

$$L_F \frac{dI_F}{dz} + M \frac{dI_L}{dz} = 0. \tag{5}$$

Also, when the L coil is turned on after ending the magnetic excitation of the F coil, which would be a natural levitation procedure, (4) can be written as

$$L_F I_{F0} = L_F I_F + M I_L, \tag{6}$$

using I_{F0}, the initial excited current of F coil when $I_L = 0$, before starting levitation.

As well as general expression of the system by equations, we will specifically see the behavior of a levitated coil by numerically calculations using example parameters. For this purpose, we choose the following coil parameters, as shown in Fig. 2. The F coil is normally located at the $z = 0$ cm plane and the current center is located at $r = 10$ cm. The current center of the L coil is at $z = 20$ cm and $z = 20$ cm. The both coils are located coaxially centered on the z axis. We assume that the F coil of $N_F = 500$ turns is excited to $I_{F0} = 100$ (A). Then current of L coil of $N_L = 100$ turns is increased to $I_L = 40$ (A) in order to levitated the F coil. Figure 2 shows magnetic field lines and field strength contours generated by these two coil currents. This is a typical magnetic field configuration of a levitated dipole experiment. Because the two currents are in a same direction, there is an X-point, or magnetic null line, between the currents.

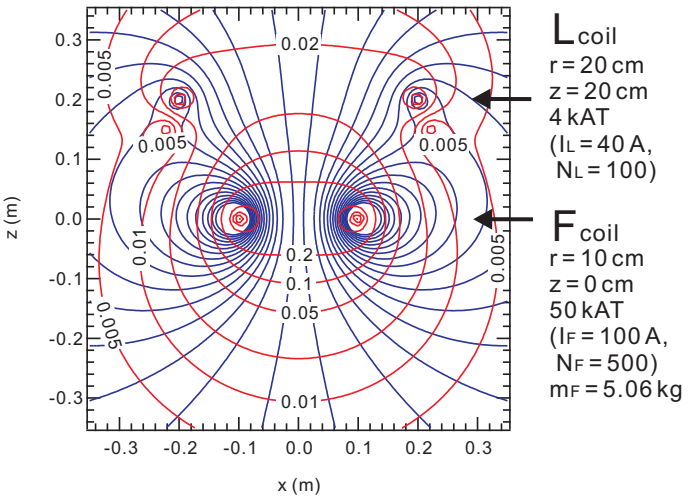

FIG. 2. Coil parameters used for equilibrium and stability calculations in the following sections. Magnetic field lines (blue) and field strength contour (red) in (T) are generated by a combination of a F and L coils.

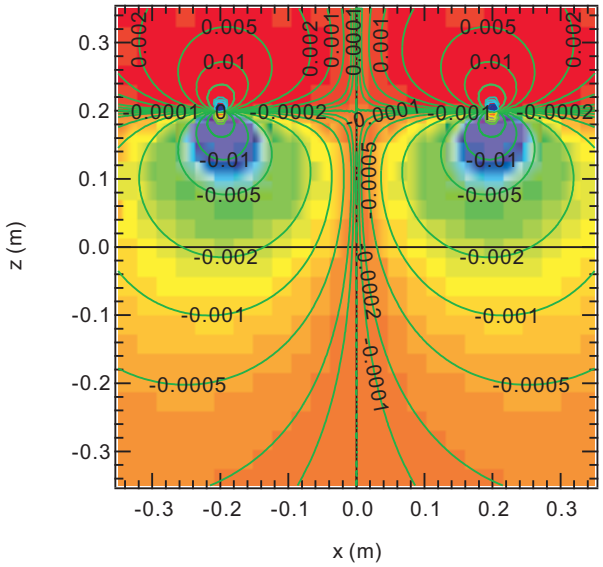

FIG. 3. Field strength contours of B_r in (T) generated by the L coil which generates levitation force of the F coil.

Coil levitation is realized by the radial component of magnetic field B_r generated by the L coil, as can be seen in Fig. 1 and (1). Here we calculate magnetic fields using a single line current approximation, which is adequately accurate for the evaluation of magnetic forces between two coils. In general, magnetic fields generated by a ring current is expressed using elliptic integrals. Here we briefly summarize these calculations. We assume that a circular coil, located at (R_c, Z_c) of I_c (A) and N_c turns, generates a magnetic field at (r, z). By using complete elliptic integral of the first and second kinds, $K(k)$

and $E(k)$, where

$$k = \sqrt{\frac{4R_c r}{(R_c+r)^2+(Z_c+z)^2}}, \tag{7}$$

magnetic field strengths are

$$B_r(r,z) = \frac{\mu_0 N_c I_c (z-Z_c)}{2\pi r\left((r+R_c)^2+(z-Z_c)^2\right)^{0.5}} \times\left(-K(k)+\frac{R_c^2+r^2+(z-Z_c)^2}{(R_c-r)^2+(z-Z_c)^2}E(k)\right), \tag{8}$$

$$B_z(r,z) = \frac{\mu_0 N_c I_c}{2\pi\left((r+R_c)^2+(z-Z_c)^2\right)^{0.5}} \times\left(-K(k)+\frac{R_c^2-r^2-(z-Z_c)^2}{(R_c-r)^2+(z-Z_c)^2}E(k)\right). \tag{9}$$

Figure 3 plots the strength of B_r that produces levitation force to the F coil. When the F coil is on the equator, $B_r(z=0) = -1.58$ mT. It means that, at $z = 0$ m, h in (3) is

$$h(z=0) = -3.95\times10^{-5}(\mathrm{T/A}). \tag{10}$$

The F coil feels an upward attractive force of $2\pi r_F N_F I_F B_r = 49.6$ N due to this B_r. This electromagnetic force is balanced by the gravity force working on the F coil of $m_F = 5.06$ kg. We will use these values, summarized in Fig. 2, for numerical calculations for the understanding of coil behavior.

Self and mutual inductances of the F and L coils are important parameters for coil behavior. The self inductance of a coil with N turns may be calculated by using a formula as a good approximation,

$$L = A\times4\pi^2\times a^2\times N^2/b\times10^{-10}\ \ (\mathrm{H}), \tag{11}$$

where $A = A(2a/b)$ is the Nagaoka coefficient, $2a$ (mm) is the major radius, and $2b$ (mm) is the minor radius of the coil. In the F coil model defined above, where $2a = 200$ mm, $2b = 30$ mm, and $N = 500$ turns, the Nagaoka coefficient is $A = 0.166$. Then

$$L_F = 0.166\times4\pi^2\times100^2\times500^2/15\times10^{-10} = 0.109\ \mathrm{H}. \tag{12}$$

Because L is very sensitive to the structure of the coil in general, the exact value of L should be decided by measurements after construction of the coil structure, in addition to the above calculations.

Mutual inductance M is defined with variation of magnetic flux inside one coil caused by current in another coil,

$$\Delta\Psi_2 = MI_1. \tag{13}$$

Because the L coil current I_L generates a magnetic flux

$$\Psi = 2\pi r A_\theta = \mu_0 N_F N_L I_L \sqrt{rR_L}\left(\left(\frac{2}{k}-k\right)K(k)-\frac{2}{k}E(k)\right) \tag{14}$$

inside the F coil loop with a radius r and vertical position z, the mutual inductance between two coils is

$$M = \mu_0 N_F N_L \sqrt{rR_L}\left(\left(\frac{2}{k}-k\right)K(k)-\frac{2}{k}E(k)\right). \tag{15}$$

In the model parameters, it is calculated to be $M = 1.61$ mH when the F coil is located at $z = 0$ cm. Basic parameters of the coil set model is summarized in Table I.

L coil	major radius	r_L	20 cm
	vertical position	z_L	20 cm
	current	I_L	40 A
	turns	N_L	100 turns
	total current	$N_L I_L$	4.0 kAT
F coil	major radius	r_F	10 cm
	normal vertical position	z_F	0 cm
	excitation current	I_F	100 A
	turns	N_F	500 turns
	total current	$N_F I_F$	50 kAT
	mass	m_F	5.06 kg
	self inductance	L_F	0.109 H
	typical mutual inductance	$M(z_F=0)$	1.61 mH
	typical h	$h(z_F=0)$	-3.95×10^{-5} T/A

TABLE I. A model coil parameters used for calculations.

B. Other useful equations for analysis

We also see several useful equations for the coil behavior analysis. In order to evaluate the stability of vertical coil motion, we define the growth rate α of a vertical magnetic force $F_{mz}(z)$, the first term of RHS of (1), against the coil motion as

$$\alpha(z) = \frac{dF_{mz}/dz}{F_{mz}} = \frac{d(I_F B_r)/dz}{I_F B_r}. \tag{16}$$

The vertical coil motion is unstable when α is positive; when the F coil moves upward toward the L coil, the F coil feels an increasing attractive force, and vice versa. This is an unstable positive feedback system. Although exact numerical calculations are done in the next subsections, we can already see from Fig. 3 that α is positive at least when ignoring the flux conservation effects (namely, assuming that $I_F = \mathrm{const.}$), indicating the need for external stabilizing mechanism.

Typical oscillation frequency of the F coil is an important system parameter toward the development of a feedback-controlled stabilizing system. For small vertical oscillation motion of the F coil near the equilibrium point of $z = 0$ cm, we may approximate that I_F is constant, assuming that we will take a so-called normal equilibrium solution among two solutions. Also by linearizing B_r, the coil oscillation motion is approximated as a harmonic oscillation in a recovering force of

$$F_{mz}(z) = -kz = -2\pi r_F I_F N_F \frac{dB_r}{dz} z. \tag{17}$$

The vertical oscillation frequency of the F coil is then

$$f = \frac{1}{2\pi}\sqrt{\frac{2\pi r_F I_F N_F}{m_F}\frac{dB_r}{dz}}. \tag{18}$$

For the above model parameters, we have $f = 1.45\,\mathrm{Hz}$. In general, it is difficult to stabilize fast oscillations using a feedback control system. This is mainly because delay times of the system, mainly decided by the response of power supplies and eddy currents, become non-negligible. Therefore there is a tendency that one may expect a stable levitation for a heavier coil, although entire system properties and safety are of course depend on many factors in addition to the characteristic frequency.

C. Equilibrium without including flux conservation effects

Before solving the above two equations, equation of motion and flux conservation law, we see the easiest equilibrium solution by using only (1), ignoring the flux conservation effects. This may correspond to a system that a permanent magnet, instead of a SC F coil, is levitated by the L coil. As shown in the next subsection, this is also a good approximation for one solution of SC F coil position including the flux conservation effects. In the equilibrium state of (2), the force balance equation is

$$2\pi r_F N_F h I_F I_L + m_F g = 0. \tag{19}$$

On stability, because I_F is constant, (16) becomes

$$\alpha(z) = \frac{dB_r/dz}{B_r}. \tag{20}$$

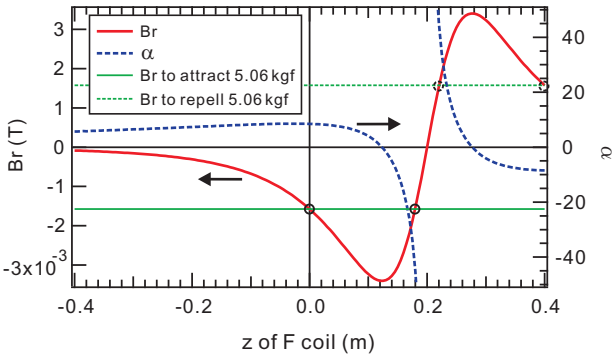

FIG. 4. Radial magnetic field B_r and growth rate α as functions of vertical position of the F coil. Circles show equilibrium points to levitate a F coil of 5.06 kg with attractive (solid thin line) and repulsive (dashed thin line) forces.

We see the coil equilibrium properties for the model parameters presented in Table I. Figure 4 plots B_r generated by the L coil, which is proportional to the levitation force on the F coil, and the magnetic force growth rate α, in variation of the F coil position. At a solution at $z = 0\,\mathrm{cm}$, $0 < \alpha$. The vertical motion of the coil is then unstable and needs a stabilization system. Because we assumed that the coil has an equilibrium point at $z = 0\,\mathrm{cm}$, we chose a system with real roots to levitate a F coil of $m_F = 5.06\,\mathrm{kg}$. In addition to this initially assumed equilibrium position at $z = 0\,\mathrm{cm}$, there is another equilibrium position at $z = 18\,\mathrm{cm}$ just below the L coil position. At this equilibrium position, the coil motion is stable against vertical motion as $\alpha < 0$. However, as discussed later, this equilibrium position is unstable against slide motions. Stated simply, the coil feels a horizontal attractive force toward the L coil, which does not happen near $z = 0\,\mathrm{cm}$, Also, coil configurations in this solution cannot make a good confinement region as far as the L coil is located outside the vacuum chamber. Because of the symmetry, there are also other solutions above the L coil position of $z = 20\,\mathrm{cm}$. There is another vertically-stable equilibrium point at $z = 40\,\mathrm{cm}$ which is realized by a repulsive force between the F and L coils. We do not use this configuration because it is not stable against slide motions in the present two-coil configuration.

For a fixed value of $m_F = 5.06\,\mathrm{kg}$ and $I_F = 100\,\mathrm{A}$, equilibrium coil currents needed for levitation is plotted in Fig. 5 for various F coil positions. Because the coil current is not affected by the flux conservation law in the present reduced mode, equilibrium current set when the F coil is at $z = 0\,\mathrm{cm}$ is

$$I_F = 100\,\mathrm{A} \quad \text{and} \quad I_L = 40.0\,\mathrm{A}. \tag{21}$$

The properties of this equilibrium for a permanent magnet is close to one equilibrium solution for a superconducting coil, as discussed in the next subsection.

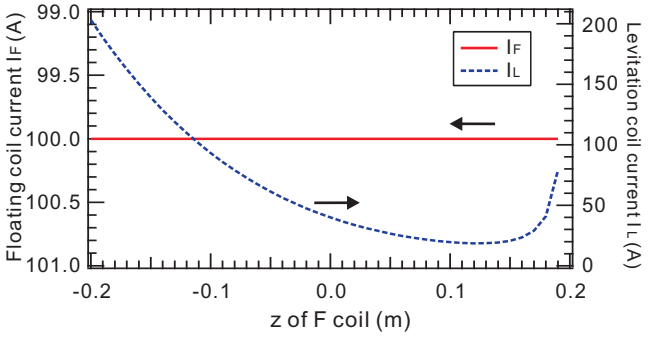

FIG. 5. Equilibrium coil currents without including flux conservation of the floating coil.

D. Equilibrium solution including flux conservation

Next we take into account the flux conservation of the SC F coil. We assume the following levitation procedure, namely, (6) is satisfied. At first, the F coil is excited to I_{F0} and mechanically supported at $z = 0\,\mathrm{cm}$, while the L coil is turned off, $I_{L0} = 0\,\mathrm{A}$. Then the L coil current is increased so that coil levitation is realized. This assumption is useful because then we can use I_{F0}, which is experimentally relatively easy to be decided routinely, as a fixed value.

By combining (19) with (6), we have

$$I_F^2 - I_{F0} I_F - \frac{m_F g M}{\pi r_F N_F h L_F} = 0, \tag{22}$$

which yields two sets of solutions,

$$I_F = \frac{I_{F0} \pm \sqrt{A}}{2} \quad \text{and} \quad I_L = \frac{L_F(I_{F0} \mp \sqrt{A})}{2M}, \tag{23}$$

where

$$A = I_{F0}^2 + \frac{2m_F g M}{\pi r_F N_F h L_F}. \tag{24}$$

When A is positive, namely the coil is not too heavy and can be levitated, the system has two equilibrium current sets for one F coil position. We call the first solution as equilibrium 1 with I_{F1} and I_{L1}, and the second solution as equilibrium 2 with I_{F2} and I_{L2}.

We can evaluate the vertical stability of these two solutions. The growth rate of the magnetic field force $\alpha = (dF_z/dz)/F_z$ is given by

$$\alpha(z) = \frac{d[h(I_{F0} - MI_L/L_F)]/dz}{h(I_{F0} - MI_L/L_F)} \tag{25}$$

$$= \frac{dh/dz}{h} - \frac{dM/dz}{I_{F0}L_F/I_L - M}. \tag{26}$$

Because the first term of (26) is often positive around $z = 0$ cm, the vertical coil motion is unstable in this region as far as this term is dominant. In the equilibrium 2, however, the second term can overcome the instability and realize stable levitation, as can be seen numerically in the following sections.

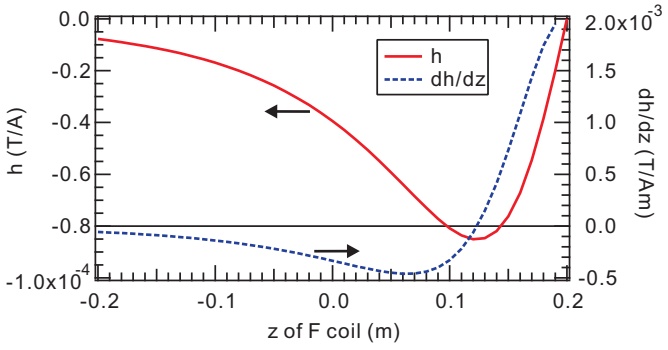

FIG. 6. Values of h, the ratio of L coil current and B_r at the F coil in (3), and dh/dz for various vertical position of the SC F magnet.

We calculate equilibrium coil currents and stability for the coil parameters in Table I. Figures 6 and 7 plot $M(z)$, $dM(z)/dz$, $h(z)$, and $dh(z)/dz$, which appear in (23) and (26), for various equilibrium F coil positions. Again we emphasize that we assumed that initially, when $I_{L0} = 0$ A, the F coil was excited to $I_{F0} = 100$ A and located at $z = 0$ cm. This is just one example of possible initial F coil positions. By using these values, I_L, I_F, and α, stability for the vertical motion, are plotted in Figs. 8 and 9 for equilibria 1 and 2. Solutions when the F coil is levitated at $z = 0$ cm are as follows. Because

$$\sqrt{A} = \sqrt{100^2 + \frac{2 \times 5.06 \times 9.8 \times 1.61 \times 10^{-3}}{\pi \times 0.1 \times 500 \times (-3.95 \times 10^{-5}) \times 0.109}} = 98.8, \tag{27}$$

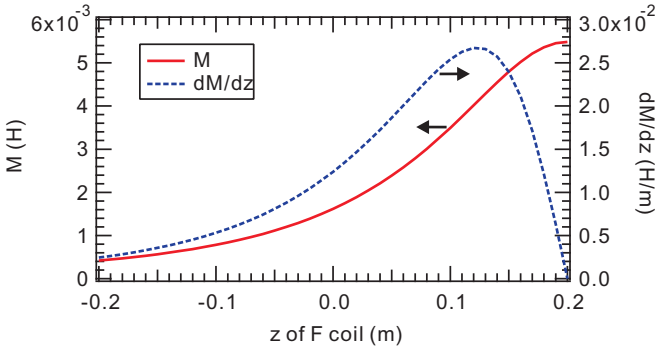

FIG. 7. Values of M, mutual inductance between the F and L coils, and dM/dz for various vertical position of the SC F magnet.

a solution in the equilibrium 1 is

$$I_F = 99.4\,\text{A} \quad \text{and} \quad I_L = 40.3\,\text{A}, \tag{28}$$

and one in the equilibrium 2 is

$$I_F = 0.6\,\text{A} \quad \text{and} \quad I_L = 6700\,\text{A}. \tag{29}$$

As shown in Figs. 8 and 9 (b), α of equilibria 1 and 2 is +8.44 (unstable) and −1260 (stable), respectively.

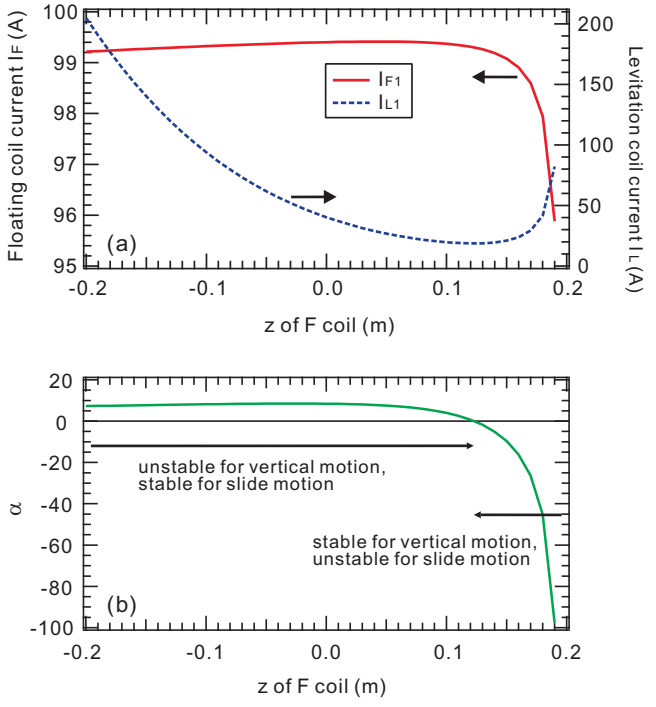

FIG. 8. Solutions of equilibrium 1 for coil parameters in Table I. (a) F and L coil current set in (23) to levitate the F coil and (b) growth rate α of (26). Around $z = 0$ cm, the coil is unstable for vertical motion as $0 < \alpha$, but is stable for slide motions.

The equilibrium 1 shown in Fig. 8, and an example is in (28), is relatively weakly affected by the the flux conservation

law of the F coil. Most of evitated dipole experiments, such as LDX, RT-1, Mini-RT, use this equilibrium. By comparing I_L curves in Fig. 8 (a) and Fig. 5, and α curves in Fig. 8 (b) and Fig. 4, we can say that this equilibrium 1 is well approximated by an equilibrium ignoring the flux conservation effects. As the SC F coil current is slightly reduced after turning on the L coil, the levitation force is compensated by slightly increased L coil current. The magnetic field configuration is quite close to the case of $I_{L0} = 40$ A and $I_{F0} = 100$ A, (21), where there are no flux conservation effects. As shown in Fig. 8 (b), this equilibrium is unstable for vertical motion and needs feedback-control system around $z = 0$ cm. In order to move the equilibrium position of the F coil downward, the L coil current must be substantially increased. At $z = -10$ cm, it is $I_L = 93.9$ A. This should be considered accordingly on the design of the actual levitation system, especially when one plans to levitate the F coil electromagnetically instead of mechanical structures. When the F coil is moved upward, we do not need larger current below $z \sim 17$ cm. However, as we will see in the next sections, slide instabilities may be unstable in this region above $z = 12.1$ cm. Because it is not easy to stabilize two-dimensional slide motions, the F coil should not approach too close to the L coil.

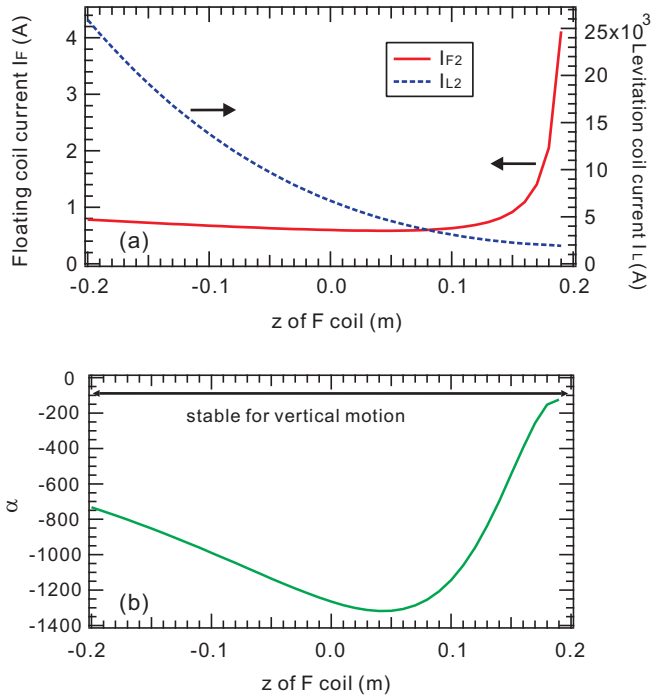

FIG. 9. Solutions of equilibrium 2 for coil parameters in Table I. (a) F and L coil current set in (23) to levitate the F coil and (b) growth rate α of (26). Because of the strong flux conservation effects, the vertical coil motion is stable without external control.

The equilibrium 2 shown in Fig. 9, whose example is (29), is quite a different solution. The persistent current of the F coil is greatly reduced, almost close to 0 when compared with the initial value of $I_{L0} = 100$ A. Still levitation is realized by very large L coil current, which mainly sustain the magnetic flux inside the F coil loop. On the stability, Fig. 9 (b) shows that this equilibrium is vertically very stable. It means that we can fix the magnet position without any external control system. This kind of stable equilibrium was experimentally demonstrated in past studies. In many plasma experiments, however, such an equilibrium is not realistic. This is because of the very large I_L (single line current exceeds 1 kA) and small confinement volume of the magnetic field configuration.

E. summary

In this section, we analyzed equilibrium and vertical stability of the F coil levitation system using an attractive force between the L coil. The levitation system has two equilibrium solutions due to the flux conservation in the superconducting loop. The first one is not strongly affected by the fluxoid conservation. In the second solution, the F coil current is greatly reduced by the flux conservation effects. Another interesting property of the second solution is its vertical stability. The flux conservation effect works as a negative feedback to the vertical F coil motion. Among the two equilibria, the first equilibrium with relatively small I_F and large I_L is more convenient than the other one, and will be used in the APEX-Dipole experiment. For this purpose, vertical motion of the F coil must be stabilized.

III. CONSIDERATIONS ON COIL STABILITIES

In the previous sections, we reviewed the stability of the coil in addition to the equilibrium solution, but it was limited to only for vertical motion. Because coil motions are three-dimensional, considerations on other modes are also needed. Otherwise stable levitation of a SC coil is not realized. In this section, we classify the entire coil motion stabilities into three categories, vertical, slide, and tilt motions, and investigate the comprehensive stability conditions. Because the slide and tilt motions are two-dimensional, detection and stabilization of these modes are not straightforward. In contrast, the vertical motion has a great advantage that it is one-dimensional motion. Therefore our basic strategy is to operate the F and L coils so that the system is spontaneously stable for the slide and tilt motion, and to stabilize the unstable vertical motion by an external feedback-control system.

A. Vertical instability

We study the vertical instability on the viewpoint of the position of F and L coils. Variation of magnetic force on a small coil segment against a vertical motion is

$$\frac{d(N_F I_F B_r)}{dz} = N_F \left(I_F \frac{dB_r}{dz} + B_r \frac{dI_F}{dz} \right). \tag{30}$$

As shown in Figs. 4 and 8, variation of I_F is relatively small, while B_r is a strong function of z in the equilibrium 1. It is a good approximation to focus only on the first term of (30).

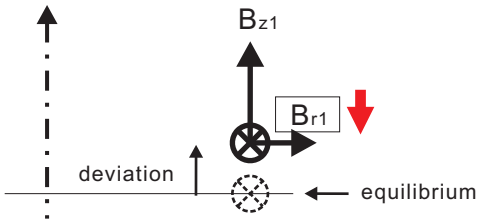

FIG. 10. Vertical deviation of the F coil from an equilibrium position and Lorentz force on the F coil in a magnetic field generated by the L coil.

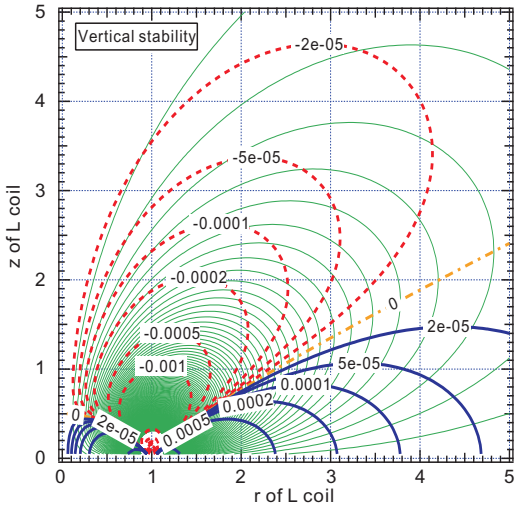

FIG. 11. Stability map for vertical motion of the F coil as functions of r and z of the L coil. The F coil is located at $r = 1$ and $z = 0$. Solid (stable) and dotted (unstable) bold lines show the contours of $\partial B_r/\partial z|_{z=0}$. Thin lines shows B_r contours.

Because the system is axisymmetric, we consider a magnetic field and Lorentz forces on one point of the F coil, as shown in Fig. 10. When there is a small vertical deviation Δz of the coil from the equilibrium ($z = 0$) position, the F coil feels the following magnetic field.

$$B_{r1} = B_{r0} + \left.\frac{\partial B_r}{\partial z}\right|_{z=0} \Delta z, \tag{31}$$

$$B_{z1} = B_{z0} + \left.\frac{\partial B_z}{\partial z}\right|_{z=0} \Delta z, \tag{32}$$

where B_{r0} and B_{z0} are values at the equilibrium point. The vertical motion is related to (31). This system is stable when

$$0 < \left.\frac{\partial B_r}{\partial z}\right|_{z=0}, \tag{33}$$

generating a restoring force for a positive deviation of Δz. It is noted that because B_r is generally negative in a system shown in Fig. 1, (33) means a decrease in the absolute value of B_r.

This condition is apparently depends on the configuration of the F and L coils. We fix the position of the SC F coil at a normalized position of $(r,z) = (1,0)$ and plot the value of the left hand side of (33) in Fig. 11. The contours in a unstable region is shown as dotted lines. The system is unstable when r_L is close to r_F. When the L coil is located near the equator of the device and, where B_r is relatively weak, there is a stable region for the vertical motion. It can be also confirmed with B_r contours, shown with thin lines in the figure.

B. Slide instability

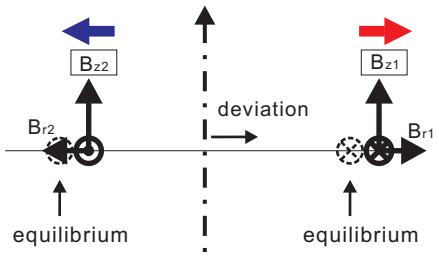

FIG. 12. Slide deviation of the F coil from an equilibrium position and Lorentz force on the F coil.

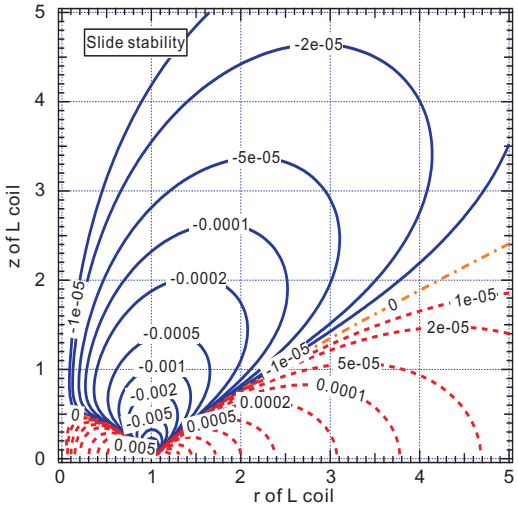

FIG. 13. Stability map for slide motions as functions of L coil position. The F coil is located at $r = 1$ and $z = 0$. Solid and dotted lines show stable and unstable regions.

Next we go to the slide instability. Due to the symmetry, we consider field strengths and forces at two symmetric points on the F coil as shown in Fig. 12. With a small position deviation Δr in a horizontal direction, the field strengths at two positions are

$$B_{r1} = B_{r0} + \left.\frac{\partial B_r}{\partial r}\right|_{z=0} \Delta z, \tag{34}$$

$$B_{z1} = B_{z0} + \left.\frac{\partial B_z}{\partial r}\right|_{z=0} \Delta z, \tag{35}$$

$$B_{r2} = B_{r0} - \left.\frac{\partial B_r}{\partial r}\right|_{z=0} \Delta z, \tag{36}$$

$$B_{z2} = B_{z0} - \left.\frac{\partial B_z}{\partial r}\right|_{z=0} \Delta z. \tag{37}$$

The slide motion is related to B_z. Assuming that the F coil current is same at positions 1 and 2, the stability condition is

$$B_{z1} < B_{z2}. \tag{38}$$

Substituting (35) and (37), we have

$$\left.\frac{\partial B_z}{\partial r}\right|_{z=0} < 0. \tag{39}$$

This condition is plotted in Fig. 12. The dotted lines are again unstable region. When compared with a case with vertical instability in Fig. 11, we see that the two instabilities are not simultaneously stabilized without using a feedback control system. While the slide instability is two dimensional, the vertical one is one dimensional. Clearly the detection and control of the instability is easy for the case of vertical instability. Therefore the L coil should be positioned with avoiding the unstable region (dotted line region in Fig. 13) of the slide instability.

C. Tilt instability

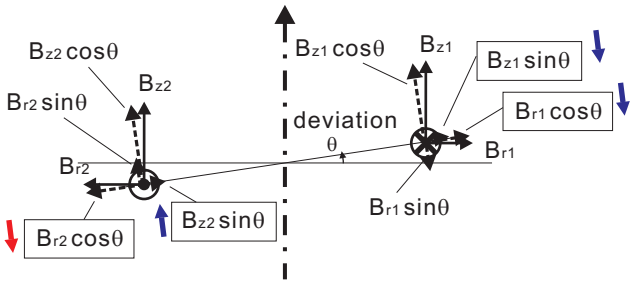

FIG. 14. Tilt deviation of the F coil from an equilibrium position and Lorentz force on the coil.

The last instability is on the tilt motion of a F coil, as shown in Fig. 14. We consider a small angle deviation from an equilibrium position and compare the field strength and forces on the coil motion. There are four forces that work as momenta for the tilt motion of the coil.

$$B_{r1}\cos\theta \sim B_{r0} + \left.\frac{\partial B_r}{\partial z}\right|_{z=0} r_F\theta, \tag{40}$$

$$B_{z1}\sin\theta \sim B_{z0}\theta, \tag{41}$$

$$B_{z2}\sin\theta \sim B_{z0}\theta, \tag{42}$$

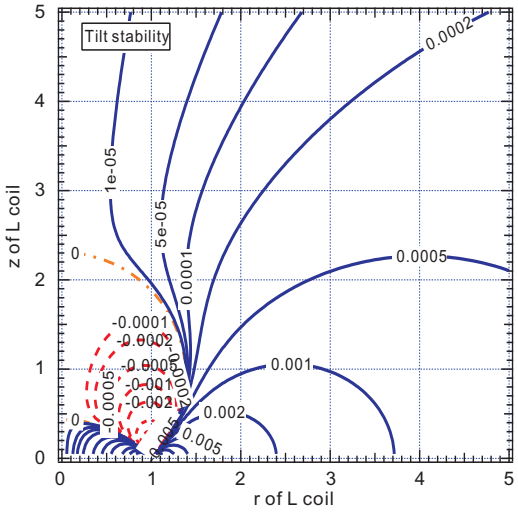

FIG. 15. Stability map for the tilt motion as functions of L coil position. The F coil is located at $r = 1$ and $z = 0$. Solid and dotted lines show stable and unstable regions.

$$B_{r2}\cos\theta \sim B_{r0} - \left.\frac{\partial B_r}{\partial z}\right|_{z=0} r_F\theta. \tag{43}$$

As shown in the figure, the stability condition is

$$B_{r2}\cos\theta < B_{r1}\cos\theta + B_{z1}\sin\theta + B_{z2}\sin\theta, \tag{44}$$

which yields

$$0 < B_{z0} + r_F \left.\frac{\partial B_r}{\partial z}\right|_{z=0}. \tag{45}$$

The tilt stability conditions is plotted in Fig. 14. It is known that this instability may be stabilized by using additional coil system. However, in the present two coils system, we can realize the tilt-stable operation of the coil by placing the L coil avoiding the dotted line region in the figure.

IV. SUMMARY OF PART I

We studied equilibrium and stability properties of a SC F coil levitated by an attractive force between a L coil located above the F coil. Among two equilibrium solutions, one with weakly affected by flux conservation effects is appropriate to be used in APEX-D. The coil behaviors strongly depend on relative positions of the F and L coils. According to linear analysis on coil motion stabilities, vertical and slide motions are alternative; we cannot stabilize or destabilize both of them simultaneously. The tilt instability also must be avoided by choosing an appropriate coil configuration. On this basis, coil position and operation conditions should be decided accordingly so that only vertical motion of the F coil will be unstable, which is stabilized by a feedback-controlled system.

Figure 16 shows a stability map for slide and tilt motions, which are not stabilized by the planned feedback-controlled system. As a position of the L coil, regions with dot lines

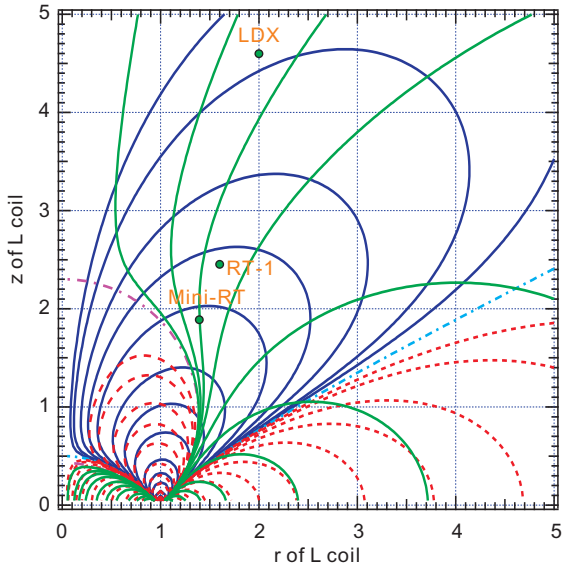

FIG. 16. Superposition of stability maps of slide and tilt motions. Dotted lines shows unstable region which should be avoided as the L coil position. The F coil is located at $r = 1$ and $z = 0$.

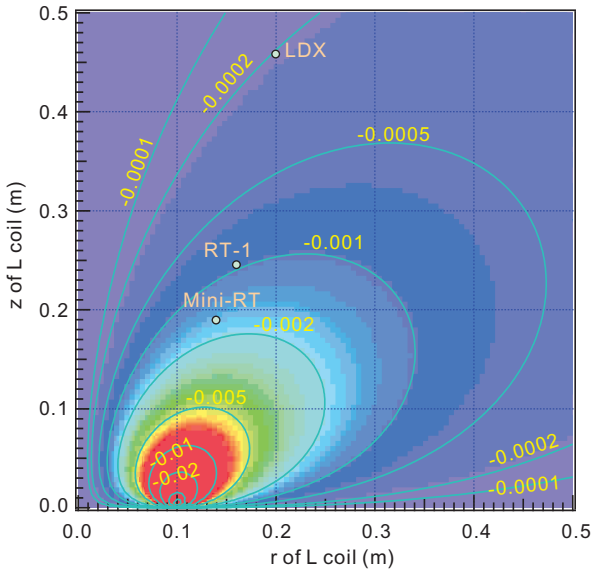

FIG. 17. Radial magnetic field at F coil position of $r = 10$ cm and $z = 0$ cm, generated by the L coil at various positions. The numbers show values of B_r (T), when the L coil current is 4.0 kAT. Circles just shows the L coil positions of previous experiments normalized by the radius of their F coil current center, and does not correspond to actual B_r values.

should be avoided. Positions of L coils in past levitated dipole experiments are plotted in the figure, all of which are located in a region with solid lines. Another important factor concerning the coil position is on the levitation force. Figure 17 plots B_r in a same manner as Fig 16, namely as functions of L coil positions. Because actual values are important, this data is not normalized and plotted in the SI unit. A new coil design and configuration will be discussed using these equilibrium and stability properties of the levitation system.

Part II: FEEDBACK CONTROL SYSTEM

V. SYSTEM ANALYSIS WITH TRANSFER FUNCTION

Through the study in Part I, now it is clear that we need a feedback controlled system to stabilize the vertical motion of the superconducting coil. In this part, we analyze the condition to stabilize the coil system using a feedback-controlled system [8]. After evaluating the stability using a transfer functions, we design a levitation circuit and demonstrate stable levitation of a permanent magnet. Basic properties of levitation and insight into the SC coil system is studied using this test experiment.

A. Methods of transfer function

The real control system, such as a magnet levitation system, often consist of combination of several components. In order to access behaviors of such a system, a transfer function is a useful mathematical representation. When a black box has an input signal $x(t)$ and an output signal $y(t)$, the transfer function is defined using their Laplace transforms,

$$G(s) = \frac{L(y(t))}{L(x(t))} = \frac{Y(s)}{X(s)}. \tag{46}$$

Here L denotes the Laplace transform. Corresponding to the functions of a black box, derivation, integration, and amplification (with a response time of T) of $x(t)$, we use the following Laplace transforms.

$$L\left(\frac{df(t)}{dt}\right) = sF(s) - f(0), \tag{47}$$

$$L\left(\int f(t)dt\right) = \frac{F(s)}{s}, \text{ and} \tag{48}$$

$$L\left(k\left(1 - e^{-t/T}\right)\right) = \frac{k/T}{s + 1/T}. \tag{49}$$

A transfer function with a form of

$$G(s) = \frac{b}{s + a}, \tag{50}$$

as shown in (49), is called a first-order delay with a response time of $T = 1/a$ and gain of $b = k/T$. For a term in the equation of motion, we also use

$$L\left(\frac{d^2 f(t)}{dt^2}\right) = s^2 F(s) - sf(0) - f'(0). \tag{51}$$

The Laplace transform is a linear transform. According to the definition, the transfer function of a series connection of

G_1 and G_1 is given by G_1G_2. That of parallel connection is given by $G_1 \pm G_2$. Owing to these characteristics, entire system properties are expressed in a simple manner by using transfer functions. Dynamics and stability of a complex system may be analyzed by well established methods in this scheme.

B. A model of coil levitation system

Figure 18 shows a typical F coil levitation system, consisting of the following components. The F coil position is detected and monitored by a laser position sensor. In actual experiments, for example in Mini-RT and RT-1, three Laser sensors are used at different toroidal positions. This is in order not to detect local tilt motions of the coil as entire vertical motions by averaging the position signal. In this analysis, however, we assume only one laser sensor for simplicity. The position signal is sent to a feedback-control circuit, which makes an output signal accordingly. This signal, which is sent to a power supply, controls the current of the L coil. There would be a time lag between the L coil current and B_r at the F coil, because of eddy currents of a vacuum chamber. The F coil responses to B_r according to the equation of motion. A flow chart of this system is shown in Fig. 19.

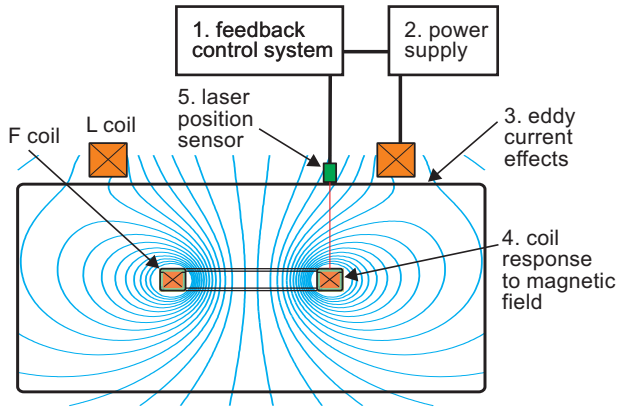

FIG. 18. Schematic of a levitation control system of a typical SC levitated dipole experiment.

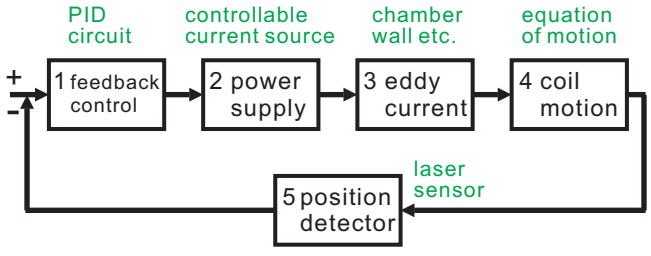

FIG. 19. Flow chart for a levitation control system in Fig. 18.

As a control circuit, we use a proportional-integral-derivative (PID) controller. In the PID controller, the input signal is sent to three components, proportional (P), integral (I), and derivative (D) circuits. Output signals from these three circuits are averaged and used as an entire output signal of the PID controller. The P circuit makes an output signal proportional to the deviation from a target value, which tries to keep the coil position uniquely. However, when the coil position is unstable, as we saw in the previous sections, the P circuit cannot solely stabilize the system. Because of the finite delay time of the system, it may make positive feedback to a position deviation, which leads to oscillation or even explosion behaviors of the system. For the stabilization of such unstable behaviors, the D circuit is important. When the coil makes a movement (not a position) such that the position deviation from the equilibrium is expected, the D circuit makes an output signal which tries to control the F coil velocity, even before the coil overshoots the equilibrium position. Thus the D circuit predicts a future position of the coil and stabilize the oscillation, which effectively work in a real system with finite delay times. The I circuit is used to moderate and improve the stabilization process, such as reducing overshoot. When the parameters of these circuit are properly adjusted, we can stabilize the system and realize stable levitation of the F coil.

The transfer function of the PID circuit is

$$G_1 = P + Ds + I\frac{1}{s}. \tag{52}$$

In magnet levitation systems, the I component is usually small and we use the following approximation.

$$G_1 \sim P + Ds = P\left(1 + \frac{D}{P}s\right). \tag{53}$$

As a power source for the L coil, we approximate the transfer function as

$$G_2 = \gamma\frac{1}{1 + s/100} \quad \text{(A/V)}. \tag{54}$$

This is a first-order transfer function with a 10 (ms) time constant. Here γ is the gain of the power source, i.e., output current (A) per input voltage (V). The eddy current effects basically work to reduce the response time of the system. Following the previous study, we assume that it is approximated as a first-order transfer function. The skin depth $\sqrt{2\rho/\omega\mu}$ of stainless steel is 1.3 cm, which would be comparable to the typical chamber wall thickness, when the frequency is 1 kHz. Here $\rho = 7\times10^{-7}$ Ωm is the electrical resistivity of stainless steel, μ is the magnetic permeability, and $f = 2\pi\omega$. Therefore one may expect that the typical delay time is in the order of 1 ms. By taking some safety margin, here we use 10 ms as a time constant. The exact value should be evaluated after construction of the chamber.

$$G_3 = \frac{1}{1 + s/100}. \tag{55}$$

The equation of motion is linearized by taking $I_L = I_{L0}(1 + I/I_{L0})$ and $h = h_0(1 + \alpha z)$ as

$$m_F\frac{d^2z}{dt^2} = -2\pi r_F N_F h_0 I_{L0}\left(1 + \frac{I}{I_{L0}} + \alpha z\right) - m_F g. \tag{56}$$

Because $-2\pi r_F N_F h_0 I_{L0} - m_F g = 0$, we have

$$m\frac{d^2z}{dt^2} = m_F g\left(\frac{I}{I_{L0}} + \alpha z\right). \quad (57)$$

By Laplace transform, this equation becomes

$$s^2 Z(s) = \frac{g}{I_{L0}} I(s) + g\alpha Z(s). \quad (58)$$

Then the transfer function of the coil motion is

$$G_4 = \frac{Z(s)}{I(s)} = \frac{1}{I_{L0}\alpha}\frac{1}{s^2/(g\alpha)-1} = \frac{1}{320}\frac{1}{s^2/78.4-1} \quad \text{(m/A)}. \quad (59)$$

Here we used $I_{L0} = 40$ and $\alpha = 8$. The response time of a laser sensor is on the order of 1 kHz, as we will see later, which is much faster than system behavior. Then we can simply write, for example for laser sensors used in RT-1,

$$G_5 = 20 \ \text{V/m}. \quad (60)$$

By combining the component 1, 2, 3, and 4,

$$G_{1-4} = P\left(1+\frac{D}{P}s\right)\times\frac{\gamma}{(1+s/100)^2}\times\frac{1}{320}\frac{1}{s^2/78.4-1} \quad (61)$$

$$= \frac{\gamma P}{320}\left(1+\frac{D}{P}s\right)\frac{1}{(1+s/100)^2(s^2/78.4-1)}. \quad (62)$$

Because the feedback component is $H = G_5 = 20$, the total transfer function of the system is

$$G_T = \frac{G_{1-4}}{1+G_{1-4}H} = \frac{\frac{\gamma P}{320}\left(1+\frac{D}{P}s\right)}{\left(1+\frac{s}{100}\right)^2\left(\frac{s^2}{78.4}-1\right)+\frac{\gamma P}{16}\left(1+\frac{D}{P}s\right)}. \quad (63)$$

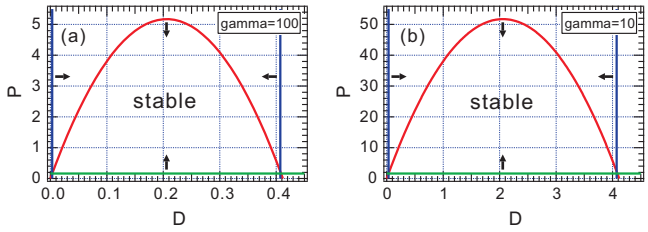

FIG. 20. Stability conditions of the levitation system for various P and D parameters of the PID feedback control circuit. Two cases of voltage-current gain, γ, are plotted.

The denominator of a transfer function is called characteristic polynomial and used to analyze the stability of a system. The characteristic polynomial of (63) is

$$\frac{s^4}{7.84\times10^5} + \frac{s^3}{3920} + \frac{s^2}{79.0} + \left(\frac{\gamma D}{16} - 0.02\right)s + \left(\frac{\gamma P}{16} - 1\right). \quad (64)$$

For (64), the characteristic equation is defined as

$$a_0 s^4 + a_1 s^3 + a_2 s^2 + a_3 s + a_4 = 0, \quad (65)$$

where $a_0 = 1.27\times10^{-6}$, $a_1 = 2.55\times10^{-4}$, $a_2 = 1.26\times10^{-2}$, $a_3 = \gamma D/16 - 2.0\times10^{-2}$, and $a_4 = \gamma P/16 - 1.0$. Solutions of a characteristic equation are called poles. In order that the system is stable, the real parts of all poles must be negative. Otherwise, i.e., when the characteristic equation has a positive pole, the step response (response of a system for input of a step function) has a divergent exponential term. Here in order to see the stability of this system, we use the Routh-Hurwitz stability criterion, which is equivalent to the above condition. According to this criterion, stability conditions of this system is to satisfy the following three equations,

$$a_n > 0, \quad (66)$$

$$\begin{vmatrix} a_1 & a_3 \\ a_0 & a_2 \end{vmatrix} = a_1 a_2 - a_0 a_3 > 0, \ \text{and} \quad (67)$$

$$\begin{vmatrix} a_1 & a_3 & 0 \\ a_0 & a_2 & a_4 \\ 0 & a_1 & a_3 \end{vmatrix} = a_1 a_2 a_3 - a_0 a_3^2 - a_1^2 a_4 > 0. \quad (68)$$

They yield

$$0.32/\gamma < D < 40.73/\gamma, \quad (69)$$

$$16/\gamma < P, \ \text{and} \quad (70)$$

$$P < -1.22\gamma D^2 + 50.24D + 0.0719/\gamma. \quad (71)$$

These conditions are plotted in Fig. 20 as functions of D and P for two different γ values. The system can be stabilized by using the D and P components feedback system, by choosing appropriate feedback parameters.

VI. DEVELOPMENT OF FEEDBACK CONTROL CIRCUIT

In this section, we develop a feedback-controlled levitation circuit with PID components, which was treated as a black box in the previous section. The feedback control circuit is applied for a test levitation system with a permanent magnet in order to demonstrate the magnet levitation and to study its properties experimentally. The test results are compared with numerical analysis.

A. Analogue feedback control circuit

A feedback control circuit was constructed with easily available and low cost analogue operational amplifiers, though it is a bit anachronistic. We used Analog Devices OP97, low-noise small-drift operational amplifiers. Figure 21 shows the circuit diagram. At present, this is a circuit for a one laser position sensor system with only one input interface. Analogue output signal form a laser position sensor is sent to U1 and U2. In future experiments, we plan to add two components similar to U1 for additional two laser sensors, using U2 as an averaging circuit for the three inputs. The output signal from

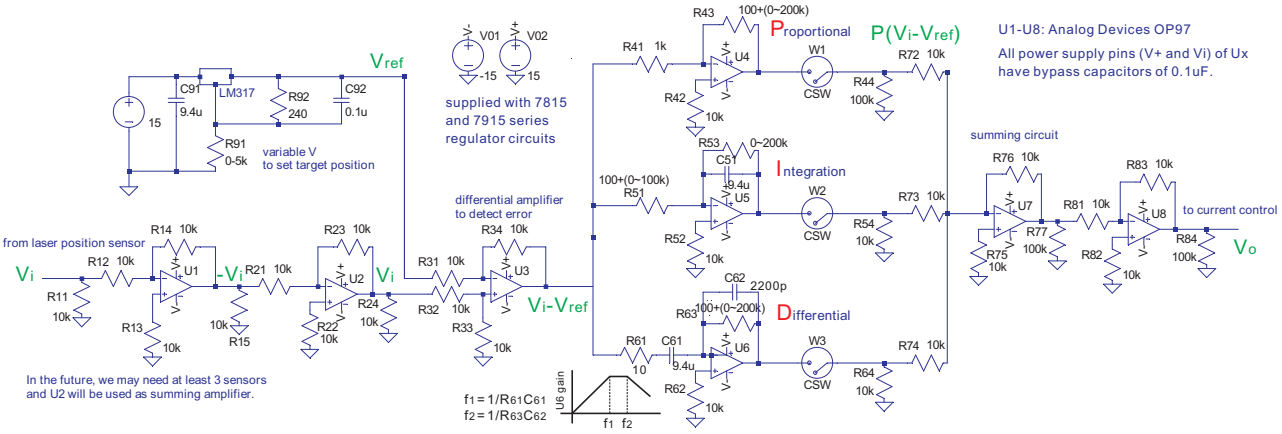

FIG. 21. PID feedback control circuit for one laser system.

U2 is sent to a differential amplifier U3, in which the output is proportional to the difference between the coil position signal and a reference signal $V_{\rm ref}$. We call this signal, $V_{\rm err} = V_{\rm i} - V_{\rm ref}$, an error signal. Here $V_{\rm ref}$ is generated by an adjustable voltage regulator, Texas Instruments LM317. The output of differential amplifier U3 is then sent to the P, I, and D circuits, which generate

$$V_{\rm P} = -\frac{R_{43}}{R_{41}} V_{\rm err}, \tag{72}$$

$$V_{\rm I} = -\frac{1}{R_{51}C_{51}} \int V_{\rm err} dt, \quad \text{and} \tag{73}$$

$$V_{\rm D} = -R_{63}C_{61}V_{\rm err}. \tag{74}$$

These signals are combined by a summing circuit U7. The output of inverter U8, $V_{\rm O}$, is used as a current control signal, which is sent to the control interface of a power supply of a F coil. The entire transfer function of this circuit is

$$G_1 = P + Ds + I\frac{1}{s} \sim P\left(1 + \frac{D}{P}s\right), \tag{75}$$

where $P = R_{43}/R_{41} < 200$ and $D = R_{63}C_{61} < 1.88$ with parameters in Fig. 21.

How the equilibrium state is realized is understood as follows. For one equilibrium coil position, the L coil current $I_{\rm L1}$ and position signal $V_{\rm i1}$ from a laser sensor are uniquely decided. As we saw in Part I, this is realized according to the equation of motion and the flux conservation law. Here two conditions, that the coil is not too heavy and the equilibrium has a real solution, and that the system can be stabilized with the used P value (for the case of Fig. 20 (a), $0.16 < P < 5.2$) must be satisfied. If the feedback-controlled circuit makes an output signal to generate $I_{\rm L1}$ for an input signal of $V_{\rm i1}$, the levitation system has a self-consistent solution. We assume that $V_{\rm i1}$ is sent to the feedback-controlled circuit. The DC component of $V_{\rm O}$ is $-P(V_{\rm i1} - V_{\rm ref})$. Because the coil current may be controlled so that it is proportional to $V_{\rm O}$, we can write it as $-\beta P(V_{\rm i1} - V_{\rm ref})$. Therefore this system has a steady state solution self-consistently, as far as we choose the values of $V_{\rm ref}$ and P so that

$$I_{\rm L1} = -\beta P(V_{\rm i1} - V_{\rm ref}) \tag{76}$$

is satisfied. In other words, the F coil is levitated at a certain point according to $V_{\rm ref}$ and P. It is noted that we can realize a solution with a same $I_{\rm L}$ value and position with various set of $V_{\rm ref}$ and P. Deviation from the equilibrium state is controlled by D and its process is adjusted by I.

There are some practical tips on the circuit. The D component circuit, U6 in Fig. 21, is not very stable and easily oscillate. In order to stabilize U6, there are R_{61} and C_{62} so that it works as a differential circuit only at low frequency ranges. In the figure, f_1 and f_2 should be much higher than the frequency range of F coil motion. On deciding the value of f_2, it should be considered that R_{63} is a variable resistance. One should also try to reduce the C component at the output of U6 between the ground. As a basic technique, multiple decoupling capacitors between supply voltages of operational amplifiers and ground will also enhance the resistance of the circuit against noise. In the present circuit, we used $0.1\,\mu$F ceramic capacitors close to V_+ and V_- pins of OP97. In order to avoid switching noises, DC voltages and $V_{\rm ref}$ are generated by series regulator based power supply circuits with IC 7815, 7819, and LM317. Also, although it was not used in the present circuit, it would be efficient to install a low-pass filter of $0.1 - 1$ kHz somewhere between the input signal of a laser sensor and U6. In any case, the D circuit would be most unstable in this circuit and its behavior should be checked by monitoring the output signal of U6.

B. Levitation test system

Using the PID feedback control circuit described above, we demonstrate stable levitation of a permanent magnet. Figure 22 shows the schematic of levitation experiment. We used a cylindrical neodymium magnet (MISUMI HXN20-3) of diameter 20 mm, height 3 mm, and weight 7 g. Including buffer

material wrapped around the magnet, the total weight was 8.4 g. Field strength at the magnet surface was 0.18 T, according to measurements with a Hall sensor probe. We can approximate this magnet as a current loop of 2990 A and diameter of 20 mm. The size and configuration of a levitation coil is shown in the figure. The levitation coil has 90 turns and operated with a current of 7 A. We approximate the levitation coil as a current loop of 630 A and diameter of 60 mm. The levitation coil current is supplied by a 10 A power supply, Elektro-Automatik PS3065-10B, which is externally controlled from its analogue interface input. The levitation test experiment is similar to that of Fig 18, but this time we have no vacuum chambers. Therefore we ignore the effects of eddy currents. The magnet position is monitored by a laser sensor, Sick OD-1, which measures a distance in a range of 50 and 150 mm. This sensor has an analogue output between 0 and 10 V proportional to the object position. Time responses of the power supply and the laser sensor is shown in Fig. 23.

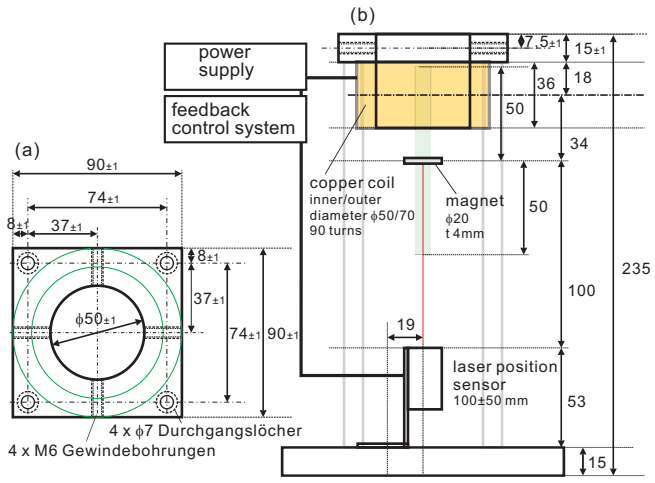

FIG. 22. Schematic of a permanent magnet levitation experiment, (a) top view and (b) side view, and levitation control system.

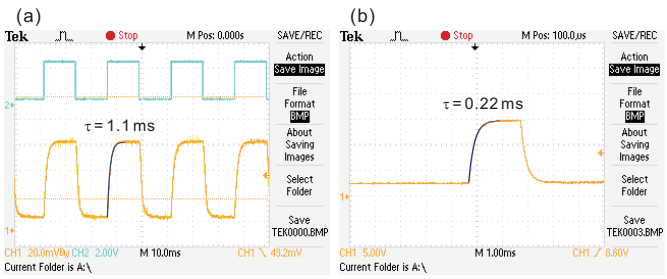

FIG. 23. (a) Time response of power supply PS3065-10B, (1) current output against (2) rectangular control voltage. A response time obtained by an exponential fitting is 1.1 ms. (b) Time response of laser position sensor OD-1. A response time obtained by an exponential fitting is 0.22 ms.

C. Stability analysis and levitation demonstration

We analyze the stability conditions of the levitation test experiment according to the previous section. We write down transfer functions of the levitation components. For the power supply, we have

$$G_2 = \frac{1}{1+s/909} \quad \text{(A/V)} \tag{77}$$

using its response time constant of 1.1 ms. Because the eddy current effects are ignored,

$$G_3 = 1. \tag{78}$$

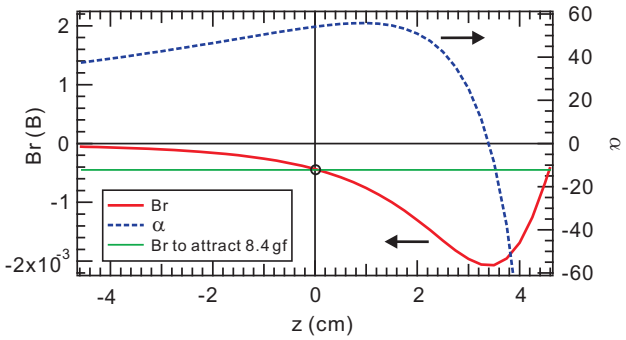

FIG. 24. B_r and α for permanent magnet levitation system. A 8.4 g magnet, located at $z = 0$ cm, is levitated by a lifting magnet centered at $z = 4.75$ cm.

According to the procedure in Sec. II C, we analyze the equilibrium of the magnet. In the present parameters, the force balance is realized when the L coil, approximated by a ring current, is located at $z = 4.75$ cm. For the motion of magnet against the magnetic field, we calculate B_r, dB_r/dz, and α numerically as shown in Fig. 24. Because $B_r = 0.436$ mT and $dB/dr = -0.0234$ T/m at $z = 0$ cm, the F coil position, $\alpha = 54.1$. Also, the L coil current was $I_{L0} = 7$ A. Therefore the transfer function (59) of the equation of motion is given by

$$G_4 = \frac{1}{I_{L0}\alpha}\frac{1}{s^2/(g\alpha)-1} = \frac{1}{379}\frac{1}{s^2/530-1} \quad \text{(V/m)}. \tag{79}$$

For the laser sensor, we include the response time of 0.22 ms and write it as

$$G_5 = 100\frac{1}{1+s/4550} \quad \text{(V/m)}. \tag{80}$$

By combining these transfer functions from G_1 to G_5, we have

$$G_T = \frac{\frac{P}{379}\left(1+\frac{D}{P}s\right)\left(1+\frac{s}{4550}\right)}{\left(1+\frac{s}{909}\right)\left(\frac{s^2}{530}-1\right)\left(1+\frac{s}{4550}\right)+\frac{100}{379}P\left(1+\frac{D}{P}s\right)} \tag{81}$$

for the entire levitation system. The characteristics equation of the system is then

$$a_0 s^4 + a_1 s^3 + a_2 s^2 + a_3 s + a_4 = 0, \tag{82}$$

where $a_0 = 4.56\times10^{-10}$, $a_1 = 2.49\times10^{-6}$, $a_2 = 1.89\times10^{-3}$, $a_3 = 0.264D - 1.32\times10^{-3}$, and $a_4 = 0.264P - 1.00$. Again by using the Routh-Hurwitz stability criterion, we have the stability conditions of the system as follows.

$$5.00\times10^{-3} < D < 39.0, \tag{83}$$

$$3.79 < P, \text{ and} \tag{84}$$

$$P < -19.4D^2 + 758D. \tag{85}$$

Lines in Fig. 25 shows these conditions.

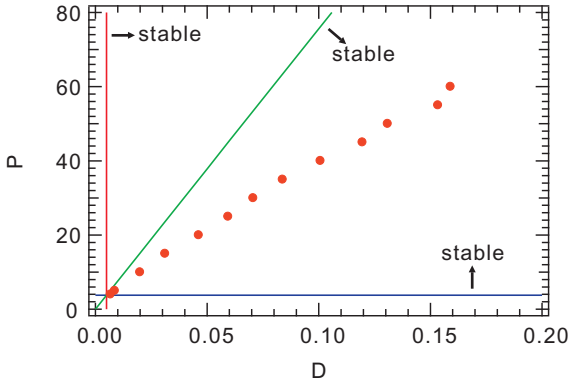

FIG. 25. Calculated stable levitation conditions in (83-85) (lines) and experimental results (circles), minimum D values needed for stable levitation.

By using this system, we tested feedback-controlled levitation of a permanent magnet. Circles in the Fig. 25 show minimum D values needed for stable levitation for various P values. We found levitation was realized only when $4.1 \le P$ and $6.6\times10^{-3} \le D$. When P was below this value, the magnet was not levitated stably with any D value. These values show fairly good agreement with (83) and (84), in spite of the use of a rather simplified analysis model. When the P and D values were close to the stability condition lines in the figure, the magnet behavior was irregular. The magnet position was often stable for a short time, but eventually vertical instability grew, which were sometimes stabilized for another short time and sometimes not. Such a non-reproductive behavior would be caused by magnetic field errors and rotation of the magnet with small structural and field asymmetry, as well as by the effects of fluctuating electromagnetic noises. As a criteria for determination of stability in this figure, we judged that the system is stable when the magnet was levitated for more than 10 s without significant fluctuations. When the D value was typically two times larger than the critical value expected by (85), the magnet was stably levitated without time constraints, as shown in Fig. 26.

As discussed in Sec. VI A, one vertical coil position of the magnet, or equivalently the L coil current, is realized with different sets of $V_{\rm ref}$ and P. We confirmed this relation in (76) with permanent magnet experiments. As shown in Fig. 21, in the present experiment $\beta = 1$. In Fig. 27, we plot values of $V_{\rm ref}$ and P for the constant L coil current of $I_{\rm L} = 7$ A, which shows good agreement with (76).

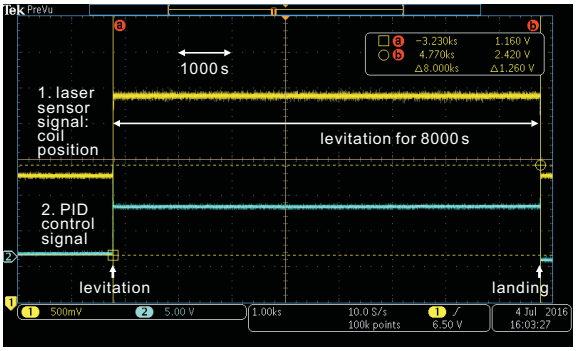

FIG. 26. Long time (8000 s) behavior of (1) laser position sensor analogue output and (2) PID control signal during levitation of a permanent magnet.

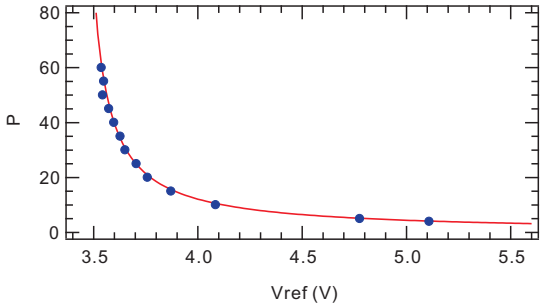

FIG. 27. Set of $V_{\rm ref}$ and P values for one equilibrium coil position. Numerical results in (76) where $\beta = 1$ (line) and experimental results (circles). The L coil current was $I_{\rm L} = 7$ A.

VII. LEVITATION SAFETY SYSTEMS

A. basic ideas

Levitation control system should have safety systems in order to reduce possibility of coil and experiment damages. The magnetic levitation system is originally unstable in vertical motion and it is externally stabilized by a control circuit. Although we assume to operate the F coil avoiding unstable regions for slide and tilt motions, such unstable regions do exist near the assumed operation region. We must be careful so that the coil system dose not unintentionally lapse into such unstable operation regions. Also, the levitation system consists of several components, whose entire functions are not very simple. The examples are behavior of laser sensors when they lose the coil positions, behavior of power supplies at electric power failure, response of the feedback-controlled circuit under strong noise environments, external magnetic fields, signal transmission failure, etc. In order to reduce unexpected accidents caused by these reasons, we should investigate possible unexpected behavior of the levitation system and consider safety mechanisms to be installed in the levitation control system.

In the previous studies, complicated safety systems, such as a coil catcher, emergency coil quench system, have been

installed. In this study, however, we hope to install simpler safety systems by taking advantages of the compact experiment.

B. Possible accidents and countermeasures

We may classify the unexpected accidents during levitation operation into three categories. The first one is dropping of the F coil. The second one is that the F coil moves upward and stick toward the L coil. The third one is large off-axis deviation of the F coil caused by slide motions.

(1) The F coil can drop by several reasons. Examples are decay of persistent current caused by increased flux-flow resistance due to coil warm up, quench of the SC coil, failure of L coil power supply and other electric equipments. In this case, the SC F coil is expected to drop onto the cooling and excitation position. The easiest solution to avoid coil damages caused by these accidents would be to make the experiment "coil droppable". Namely, to design it so that the F coil can drop from a normal levitation position to a cooling position safely, at least for several times. This would be realized by minimizing the levitation distance and making the F coil with enough mechanical strengths. We should study the structures of field lines and SC coil support carefully, so that the levitation distance becomes as short as possible. Also, it may be possible to absorb drop impact by using some dumper structures at the cooling point or at the coil case itself. The RT-1 device has a safety coil catcher system located 10 cm below the normal coil position, which opens quickly in emergency cases. Thus we may expect that 10 cm is an acceptable drop distance on the SC coil side. In order to avoid coil drop caused by the decrease of persistent current, there should be a monitor system for L coil current. When the L coil current exceeds a certain value, we can judge that current decay is significant and try to safely land the F coil.

(2) Once a F coil moves upward and sticks to the top of the vacuum chamber, recovery of the coil is very difficult. This can happen by an error response of laser position sensors, failure of levitation control circuit, etc. By turning off the L coil current, or after decay of the persistent current, the F coil would drop toward the chamber bottom. However, because the dropping distance is much longer than the above case 1, more serious damage is expected. Also, there is a slide-motion unstable region near the L coil. Therefore we should have a safety system to restrict the vertical F coil position below a certain vertical position. Such a mechanism may be realized by installing a circuit to set an upper limit value of the L coil current, according to a manual set position or laser sensor signals. It is noted that this kind of safety system can unintentionally work when the persistent current decays considerably. As well as the current limiter, we should also have an independent emergency current stopping circuits solely for the L coil power supply.

(3) We expect that the above mechanisms 2 would work efficiently in order not to operate the F coil in slide-unstable regions. We can also install a center stack and use it as a guide rail for vertical motion of the F coil, which also can be used as a bias electrode.

VIII. SUMMARY OF PART II

In this part, we studied a feedback-controlled coil levitation system for a levitated dipole experiment. The system stability was analyzed by a simple model using transfer functions, which include finite time responses of system components, as well as equation of motion and flux conservation law for a superconducting F coil. After showing the existence of stable region, we constructed a PID feedback control system using conventional analogue circuits. We applied this PID circuit to a test levitation system with a permanent magnet. The results demonstrated the validity of the analysis and feedback-controlled system itself, which can be also used in future experiments with a SC F coil.

[1] T. Sunn Pedersen, J. R. Danielson, C. Hugenschmidt, G. Marx, X. Sarasola, F. Schauer, L. Schweikhard, C. M. Surko, and E. Winkler, New J. Physics **14**, 035010 (2012).

[2] A. Hasegawa, Comments Plasma Phys. Control. Fusion **11**, 147 (1987).

[3] S. Mizumaki, T. Tosaka, Y. Ohtani, M. Ono, T. Kuriyama, K. Nakamoto, M. Shibui, N. Tachikawa, S. Ioka, J. Morikawa, Y. Ogawa, and Z. Yoshida, IEEE Trans. Appl. Supercond. **16**, 918 (2006).

[4] Y. Yano, Z. Yoshida, Y. Ogawa, J. Morikawa, and H. Saitoh, Fusion Eng. Design **85**, 641 (2010).

[5] Z. Yoshida, H. Saitoh, Y. Yano, H. Mikami, N. Kasaoka, W. Sakamoto, J. Morikawa, M. Furukawa, and S. M. Mahajan, Plasma Phys. Control. Fusion **55**, 014018 (2013).

[6] M. Nishiura, Z. Yoshida, H. Saitoh, Y. Yano, Y.Kawazura, T. Nogami, M. Yamasaki, T. Mushiake, and A. Kashyap, Nucl. Fusion **55**, 053019 (2015).

[7] A. C. Boxer, R. Bergmann, J. L. Ellsworth, D. T. Garnier, J. Kesner, M. E. Mauel, and P. Woskov, Nat. Phys. **6**, 207 (2010).

[8] J. Morikawa, D. Ozawa, Y. Ogawa, N. Yanagi, S. Hamaguchi, and T. Mito, Jpn. J. Appl. Phys. **40**, L1029 (2001).